

# Swelling-induced volumetric strains internal to a stressed coal associated with CO<sub>2</sub> sorption

C. Özgen Karacan

*National Institute for Occupational Safety and Health, Pittsburgh Research Laboratory, Pittsburgh, PA, United States*

## Abstract

It is generally accepted that typical coalbed gases (methane and carbon dioxide) are sorbed (both adsorbed and absorbed) in the coal matrix causing it to swell and resulting in local stress and strain variations in a coalbed confined under overburden pressure. The swelling, interactions of gases within the coal matrix and the resultant changes in the permeability, sorption, gas flow mechanics in the reservoir, and stress state of the coal can impact a number of reservoir-related factors. These include effective production of coalbed methane, degasification of future mining areas by drilling horizontal and vertical degasification wells, injection of CO<sub>2</sub> as an enhanced coalbed methane recovery technique, and concurrent CO<sub>2</sub> sequestration. Such information can also provide an understanding of the mechanisms behind gas outbursts in underground coal mines.

The spatio-temporal volumetric strains in a consolidated Pittsburgh seam coal sample were evaluated while both confining pressure and carbon dioxide (CO<sub>2</sub>) pore pressure were increased to keep a constant positive effective stress on the sample. The changes internal to the sample were evaluated by maps of density and atomic number determined by dual-energy X-ray computed tomography (X-ray CT). Early-time images, as soon as CO<sub>2</sub> was introduced, were also used to calculate the macroporosity in the coal sample. Scanning electron microscopy (SEM) and photographic images of the polished section of the coal sample at X-ray CT image location were used to identify the microlithotypes and microstructures.

The CO<sub>2</sub> sorption-associated swelling and volumetric strains in consolidated coal under constant effective stress are heterogeneous processes depending on the lithotypes present. In the time scale of the experiment, vitrite showed the highest degree of swelling due to dissolution of CO<sub>2</sub>, while the clay (kaolinite) and inertite region was compressed in response. The volumetric strains associated with swelling and compression were between  $\pm 15\%$  depending on the location. Although the effective stress on the sample was constant, it varied within the sample as a result of the internal stresses created by gas sorption-related structural changes. SEM images and porosity calculations revealed that the kaolinite and inertite bearing layer was highly porous, which enabled the fastest CO<sub>2</sub> uptake and the highest degree of compression.

*Keywords:* Coal; Carbon dioxide; Sorption; Swelling; Sequestration; X-ray computed tomography; Volumetric strain; Gas outbursts

## 1. Introduction

Sorption of typical coalbed gases (methane and carbon dioxide) in the coal matrix forces it to swell, resulting in localized stress and strain variations in a coalbed confined under overburden pressure. Such changes impact

commercial production of coalbed methane, potential degasification of future mining areas by drilling horizontal and vertical degasification wells, enhanced methane recovery using CO<sub>2</sub> injection, and concurrent sequestration of CO<sub>2</sub>. Such knowledge can also provide an understanding of the mechanisms leading to gas outbursts in underground coal mines.

The presence of large amounts of carbon dioxide in a coalbed due to coalification, hydrodynamics, igneous activity, or as a result of injection is particularly important. Carbon dioxide has a greater affinity towards coal than methane and is not only adsorbed on the coal surface, but is also dissolved in the coal matrix (Karacan, 2003; Larsen, 2004) like an organic liquid. This process modifies the physical structure of the coal matrix and may even extract some of the polycyclic aromatic hydrocarbons and mobilize them in the coalbed (Kolak and Burruss, 2006). The modification in physical structure is associated with a relaxation and rearrangement of the macromolecular structure of the coal. The presence of CO<sub>2</sub> produces a greater change in the initial pore structure (Larsen, 2004) than does the presence of methane. One impact of CO<sub>2</sub> interaction with coal may be more violent and difficult-to-control gas outbursts, when compared to those caused by methane alone (Lama and Saghafi, 2002). CO<sub>2</sub> injection, with concurrent production of methane, can cause swelling of the coalbed particularly in the near wellbore area and a change in its permeability, a factor which limits the development and potential field application of this technology (Reeves, 2003). Coal swelling affects the accuracy of gas adsorption measurements in the laboratory, too. Since coal swelling is dependent on the CO<sub>2</sub> pressure, both coal surface area and the error due to coal swelling will change with CO<sub>2</sub> pressure (Özdemir et al., 2003; Romanov et al., 2006a,b).

The molecular rearrangement of coal caused by molecules dissolving in the coal can be explained by classical polymer chemistry. Coals are glassy, strained, cross-linked macromolecular systems that are not at their lowest energy state (Larsen et al., 1997). The brittleness of coals is due to their glassy structure, which has intramolecular interactions greater than the available thermal energy, and the molecules have limited freedom to move except for some small-scale vibrations and rotations. When the coal interacts with a solvent, the free volume of the polymeric system increases and lowers  $T_g$  (glass transition temperature), the temperature at which the glass becomes a rubber. For coals having less than about 85% C, the rearrangement of coal molecules is towards a more highly associated structure in which the solubility of liquids is reduced, sometimes by one-half.

This suggests that under long-term storage or injection conditions with CO<sub>2</sub> absorbed in a coal, the coal undergoes a slow rearrangement that will decrease the solubility of this gas, expelling it from the structure. The situation with coals having C levels in excess of 85% is more complicated. Thus, it would not be surprising to expect different rearrangements, sorption, and rate behaviors when the coal rank changes.

Karacan (2003) showed the heterogeneous character of CO<sub>2</sub>-coal interactions and the behavior of different microlithotypes within the coal. The study showed that vitrite, liptite, and clarite densities decreased with increasing gas pressure. The results indicated dissolution of CO<sub>2</sub> in coal, which created some free volume so that the macromolecular structure of the coal could relax or swell on the time scale of the experiment. The density change kinetics of vitrites, liptite, and clarite showed a “breathing” (expansion-contraction) behavior, during which the density bounced back by expulsion of excess CO<sub>2</sub> revealing an “overshoot” swelling behavior, a similar phenomenon that was observed before by Gao et al. (1999) on a bituminous coal. This phenomenon was caused by the diffusion and solution of gas molecules in the macromolecular structure of mainly vitrites, followed by subsequent swelling and then rearrangement to a more highly associated structure.

The changes in Pittsburgh No. 8 coal structure caused by CO<sub>2</sub> sorption and the mechanism of diffusion were studied by Goodman et al. (2005). They measured the sorption of CO<sub>2</sub> using a high pressure ATR-FTIR (attenuated total reflectance-Fourier transform infrared) spectrometer. They demonstrated that after the first sorption at 55 °C and 0.35 MPa, subsequent sorption was much faster, indicating that structural changes in the coal occurred after the first sorption. They also noted that the rearrangement was not reversed as CO<sub>2</sub> was removed from the coal. They concluded that CO<sub>2</sub> plasticized the coals and changed subsequent diffusion rates, adsorption isotherms, and solubilities.

It has been shown that coals possess anisotropic behavior in swelling and the degree of swelling rate is larger perpendicular to the bedding plane, compared to parallel to the bedding plane, where bond density is lowest (Cody et al., 1988; Ceglarska-Stefanska and Czaplinski, 1993; Larsen et al., 1997). This behavior and the anisotropic structure of coal have been attributed to the stress conditions under which the coal was generated (Cody et al., 1988). Majewska and Zietek (in press) observed the anisotropic swelling of cylindrical coal samples subjected to sorption-desorption cycle using CO<sub>2</sub> by employing strain gauges and acoustic transducers.

Evaluation of the degree of swelling at particular thermodynamic conditions is important since significant coal matrix swelling can affect various processes. In the case of CO<sub>2</sub>, significant swelling or volume increases ranging from 0.75% to 4.18% were observed in a range of coal samples when they were exposed to CO<sub>2</sub> at pressures up to 1.5 MPa (Reucroft and Sethuraman, 1987). Increases in pressure produced increases in swelling and a decrease in the time required to reach maximum swelling. Robertson and Christiansen (2005) found a linear strain of less than 1.0% in CO<sub>2</sub> for pressures up to 5.3 MPa using optical techniques. Their linear strain for a sub bituminous coal was 2.1%, which was more than for a bituminous coal. Levine (1996) measured a swelling ratio of 0.41% at 3.1 MPa for bituminous coal samples from Illinois. He suggested that the swelling function was similar to the Langmuir isotherm. Harpalani and Chen (1995) found a linear relation between the coal matrix volumetric strain and the quantity of gas desorbed. Majewska and Zietek (in press) reported volumetric strains up to 16% on a bituminous coal sample from Poland during sorption of CO<sub>2</sub> at 4 MPa. Different volumetric strain measurements in different studies may be related to factors such as sample composition, experimental method, sample size, and the temperature of the experiment.

The swelling process may play an important role in determining the strength of a coal, the speed at which a coal can absorb additional gas, and the impact of permeability changes on the gas flow mechanics in the coalbed reservoir. These are important factors for evaluating the long-term effects of CO<sub>2</sub> injection into a reservoir for sequestration, for assessing the integrity of well completions, and for understanding the mechanics of violent CO<sub>2</sub>-associated outbursts in coal mines. Beamish and Crosdale (1998) listed major outburst incidents in the world. The incidents are usually coincident with the gassy seams in Australia, in Europe and in China and most of them are originated either purely from CO<sub>2</sub> or from CH<sub>4</sub>/CO<sub>2</sub> gases combined. Outbursts, besides the degree of shearing of the coal, are associated with coals of high gas contents, low permeabilities that lead to high gas pressures, low mechanical strength, and high stress levels in the seam (Lama and Saghafi, 2002; Li and Shimada, 2003) which are all conditions arising from swelling of the coal matrix. In another instance, CO<sub>2</sub> injectivity in the Allison Unit (Reeves, 2003) decreased because of reduced near-wellbore permeabilities, possibly due to matrix swelling and reductions in cleat porosity and permeability. Thus, estimations of coal swelling are important for evaluating coalbed behavior. Currently, the most widely used predictive

technique to describe porosity changes as a result of gas sorption and relating those changes to permeability is the Palmer and Mansoori model (1998). Recently, Pan and Connell (2007) proposed a predictive surface energy–elastic energy balance approach to describe swelling and shrinkage of coal matrix as a result of gas adsorption by using theoretical and experimental parameters. Although the model predicts swelling data reasonably well using literature data, it does not include the thermodynamics of polymeric behavior. Thus, it assumes that swelling occurs as a result of only surface forces, which may be an invalid assumption for coal–CO<sub>2</sub> systems.

This study presents an evaluation of swelling-induced volumetric strains occurring internal to a stressed coal subjected to CO<sub>2</sub> pressure. The evaluation is based on calculations using the quantitative, time-resolved spatial maps of coal density and mass percentage of sorbed CO<sub>2</sub> in the coal derived from effective atomic number computations. The data are presented as swelling/compaction maps and values along profiles. SEM (scanning electron microscopy) images of different locations of interest were taken to interpret the observed behavior. The aim of this study is to document the swelling behavior of a confined and stressed coal under CO<sub>2</sub> exposure and to identify the behaviors of different microlithotypes.

## 2. Experimental

Karacan (2003) has provided a more in-depth overview of the experimental technique used in this study. However, the approach and some relevant details to the present study will be summarized here.

### 2.1. CO<sub>2</sub> sorption experiment

A high volatile bituminous coal from the Pittsburgh seam (DECS-12) was cored parallel to the bedding planes to obtain a cylindrical sample (2.5 cm in diameter and 2.0 cm long). The average elemental composition of the sample was: 74.78% C, 5.11% H, 1.23% N, 1.12% S, and 7.51% O. The sample had 2.5% moisture as received and 10.25% ash in proximate analysis.

The CO<sub>2</sub> sorption experiment was conducted in a biaxial pressure cell made up of aluminum, which is capable of applying CO<sub>2</sub> gas pressure and confining pressure to the sample separately. The pressure cell containing the sample was placed on the computer-controlled table of a fourth-generation medical X-ray CT scanner, which was capable of producing a single-energy-level scan in 4 s. The pixel resolution and the

image thickness were 0.25 mm and 2.0 mm, respectively. During this study, the sample was scanned at two energy levels: 130 kV and 80 kV with an X-ray intensity of 65 mA. The  $512 \times 512$  images generated by the scanner were later cropped to construct  $100 \times 100$  data matrices focusing only on the coal.

The pressure history of the experiment was as follows. Initially, confining pressure on the sample was set to 1.36 MPa, which was the effective pressure on the sample that would be kept constant throughout the experiment. The sample was scanned to establish the condition of the sample under vacuum but with the 1.36 MPa confining pressure. The sample was pressurized with 1.70 MPa CO<sub>2</sub>, while increasing the confining pressure to 3.06 MPa. The sample was scanned until equilibrium, which took approximately 7240 min. The next sorption pressure and confining pressure were 3.06 MPa and 4.42 MPa, respectively. As before, the sample was scanned for another 7240 min. The procedure was repeated for 4.42 MPa gas pressure and 5.78 MPa confining pressure for the last 5000-minute period. This experimental methodology enabled the experiment to be conducted at three different gas pressures while keeping the sample under constant effective stress.

After the experiment, the coal sample was recovered from the core holder, vacuum impregnated with a cold-setting epoxy resin, and cut at the approximate spot of CT-scan location. The sample was ground and polished to analyze the surface by using the 20-point ocular procedure defined by the [International Committee for Coal Petrology \(1963\)](#). A more detailed explanation of this procedure is given in [Karacan and Mitchell \(2003\)](#).

The polished surface was later coated with carbon to analyze the locations of interest by SEM using a 20 kV electron beam and different magnifications. EDX (Energy Dispersive X-ray) analysis coupled with the SEM system was used to identify the elements present at points of interest.

## 2.2. Processing of dual-energy images

Dual-energy X-ray scanning enables the independent determination of density and composition from CT data and thus enables the quantitative investigation of the material while using two different beam energy spectra (high: h and low: l) to distinguish the effects of different components in mixtures:

$$\rho(x, y) = \frac{b_h \mu_l(x, y) - b_l \mu_h(x, y)}{b_h a_l - b_l a_h} \quad (1)$$

$$Z_e(x, y) = 3.8 \sqrt{\frac{a_l \mu_h(x, y) - a_h \mu_l(x, y)}{b_h \mu_l(x, y) - b_l \mu_h(x, y)}} \quad (2)$$

In these equations  $a$  and  $b$  are energy-dependent constants. Calibrating the scanner readings with materials of known density and effective atomic number enables bulk density ( $\rho$ ) and effective atomic number ( $Z_e$ ) maps of the scanned object to be generated at each pixel position  $(x, y)$  independently using linear attenuation of X-rays ( $\mu$ ) by solving for the energy-dependent constants.

For mixtures of atoms, an effective atomic number ( $Z_e$ ) is used instead of  $Z$ . The relevant literature features various definitions of effective atomic number. [Schät-zler \(1979\)](#) proposed a formula where the atomic number of each element is weighted by the mass percentage,  $\omega_i$ , of each element:

$$Z_e = \sum_i \omega_i Z_i \quad (3)$$

In order to map the mass percentage of CO<sub>2</sub> at any location, temporal effective atomic number maps were used. For this purpose, the effective atomic number of CO<sub>2</sub> and the spatial distribution of effective atomic number of the initial coal matrix were considered as simple elements with  $Z_e$  electrons per atom ([Duvauchelle et al., 1999](#)). This established an analogy with the classical atomic model and the use of Eq. (3) to calculate the mass percentages of CO<sub>2</sub> at any given time during CO<sub>2</sub> sorption.

By using the relation given in Eq. (4) and the temporal and spatial distribution of effective atomic number of coal (Eq. (2)) for each scan time, we can obtain the mass percentage of CO<sub>2</sub> in the coal using Eq. (5).

$$Z_e(x, y) = \sum_i \omega_i(x, y) Z_i(x, y) \quad (4)$$

$$\omega_{\text{CO}_2}(x, y) = \frac{Z_{e@t}(x, y) - Z_{\text{coal\_initial}}(x, y)}{Z_{\text{CO}_2} - Z_{\text{coal\_initial}}(x, y)} \quad (5)$$

In this equation,  $Z_{e@t}(x, y)$  is the temporal effective atomic number map of coal at pixel location  $(x, y)$ ,  $\omega_{\text{CO}_2}(x, y)$  is the mass percentage CO<sub>2</sub>,  $Z_{\text{CO}_2}$  is the effective atomic number of CO<sub>2</sub> (7.581), and  $Z_{\text{coal\_initial}}(x, y)$  is the effective atomic number of the initial coal material before sorption of CO<sub>2</sub>. The images were processed by using the programs written in PV-WAVE command language.

### 3. Results and discussion

#### 3.1. Sample characterization

Visual analysis of the sample showed varying bands of bright and dull layers of varying thicknesses and mineral bands. However, it is apparent from Fig. 1 that one side of the sample can be characterized more by a dull, high-mineral-matter containing region (light colors), which was highly concentrated with clays and inertite type microlithotypes, compared to the other side of the sample, which contained thicker and more persistent bright layers (darker colors in Fig. 1), mainly rich in vitrite and clarite. Microlithotype analyses using a 20-point ocular procedure defined by the International Committee for Coal Petrology (1963) showed that the sample had about 32.0% vitrite, 1.2% inertite, 28.5% clarite, 10.2% vitrinertite, 8.3% duroclarite, 1.3% clorodurite, 7.4% partings, 9.4% carboargilite, and 1.9% carbopyrite.

Microlithotypes at some specific locations were also identified using petrographic analysis. These locations are shown in Fig. 1, and the identifications are listed in Table 1.

#### 3.2. Mapping of macroporosity

X-ray attenuation is linearly additive for a composite material such that the fractional contributions from the

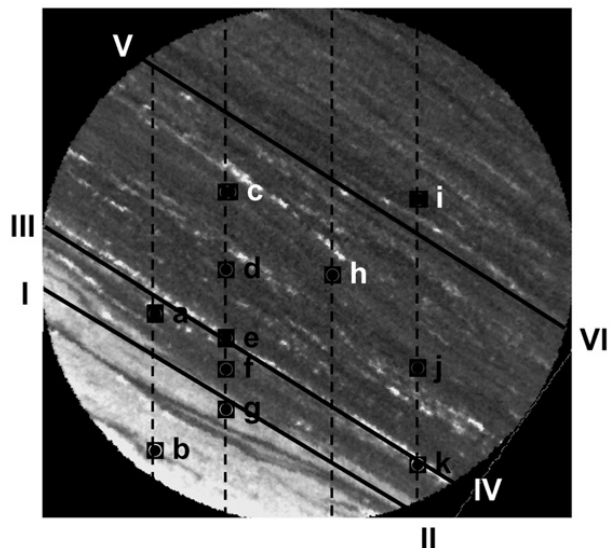


Fig. 1. A micro-focus X-ray tomography image showing the internal structure of coal sample at the scan location. Bright layers are higher density, clay and rock layers whereas darker layers are organic lithotypes of varying macerals. The figure also shows various locations whose microlithotype identification was documented in Table 1. Straight, diagonal lines are the profiles along which macroporosity values are shown in Fig. 2.

Table 1

Microlithotypes determined at the positions shown in Fig. 1

| Location | Microlithotype   |
|----------|--|
| a        | Pyrite particles in a matrix of resinite matrix                                  |
| b        | Mineral parting and carbargilite   |
| c        | Vitrite  |
| d        | Vitrite and clarite  |
| e        | Pyrite layer in a matrix of liptite  |
| f        | Pyrite particles in a matrix of resinite and other liptite macerals, and vitrite |
| g        | Clay and inertite  |
| h        | Vitrite, inertite and liptite  |
| I        | Clarite, cutinite and vitrinertite   |
| j        | N/a  |
| k        | N/a  |

attenuation coefficients of each of the pure materials give the total attenuation. This property helps to calculate the porosity in each voxel from images taken at a single energy level. The conventional method of calculating porosity with single-energy CT scanning is to saturate the pore space with two different fluids and determine the change in attenuation of X-rays in the sample due to the presence of these two fluids in pore volume.

For calculating the voxel-resolved local macroporosity distribution within the coal sample at the X-ray CT-scan location, the scans taken before,  $CT_{t0}$ , and immediately after,  $CT_{t1}$ , introducing 1.70 MPa  $CO_2$  were used as the sample was under 1.36 MPa effective stress. The following equation was used for this calculation:

$$\phi(x, y) = \frac{CT_{t1}(x, y) - CT_{t0}(x, y)}{CT_{CO_2} - CT_{air}} \quad (6)$$

In this equation  $CT_{CO_2}$  and  $CT_{air}$  are the CT numbers (a quantity in Hounsfield units representing the attenuation of X-rays) of pure  $CO_2$  and air filling the macropore space, respectively. CT numbers of  $CO_2$  and air were determined by scanning the free gas phase that was in the calibration phantom placed in the sample cell for this purpose. The CT numbers determined as such were  $-835$  for air and  $-655$  for  $CO_2$  (at 1.7 MPa), respectively.

Macroporosity data have been extracted along the profiles I–II, III–IV, and V–VI, shown in Fig. 1. According to the microlithotype identification, profile I–II is mainly along the clay and inertinite band, profile III–IV is along the liptite layer with pyrite and mineral inclusions, and V–VI is within the clarite and vitrite layers.

Results of the porosity analysis showed that the microlithotypes with maceral compositions that were rich in inertinite, mineral, or clay had higher porosities compared to the microlithotypes rich in vitrite and liptite. Depending on the location along I–II profile, the porosity values changed between 2% and 12% (Fig. 2-A). In the section where the profile is completely within the band (Fig. 1), the value is approximately 12% and is probably more representative for clay and inertite, both known to be porous materials. This was confirmed by SEM images taken at this section (Fig. 3-A and B). SEM images show

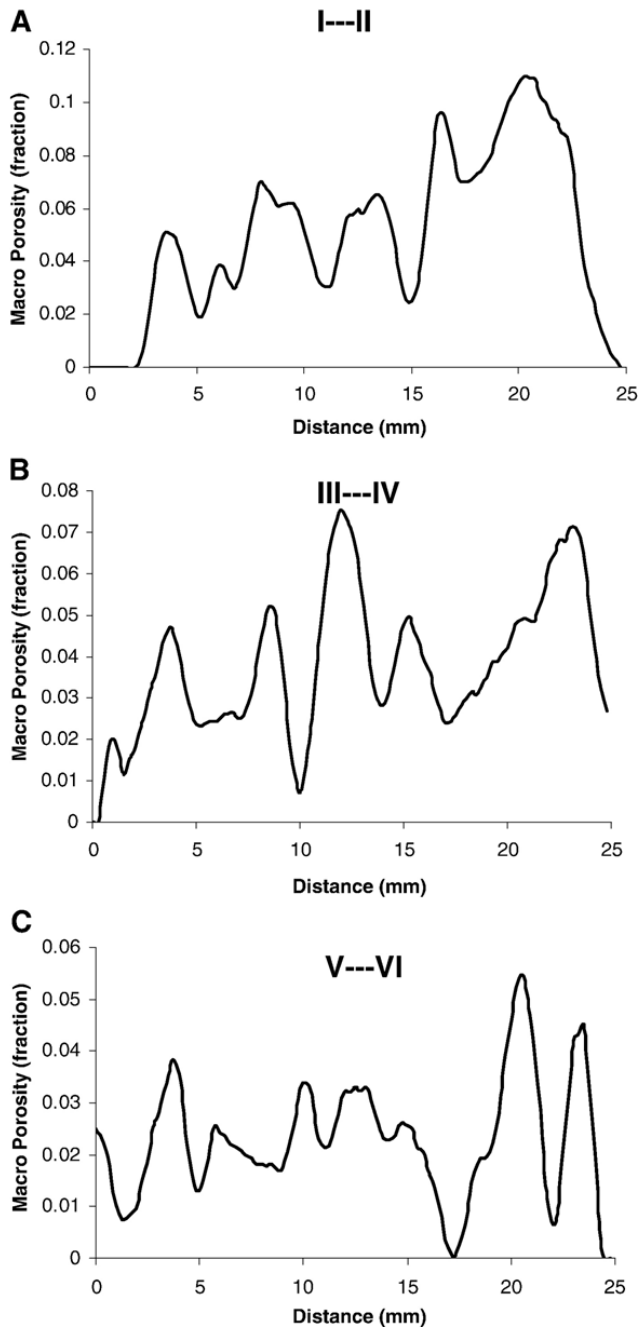


Fig. 2. Macroporosity of the coal determined by computer tomography method along profiles, A: I–II, B: III–IV and C: V–VI, shown in Fig. 1.

that the porosity is mainly formed by either large openings or as spaces between the flaky clay sheets. EDX scans taken on the magnified image (Fig. 3-B) show that the average elemental composition is 55.5% O, 13.0% Al, and 28.0% Si and minor amounts of K, Fe, and Mg. These compositional data suggest that the clay is either kaolinite or kaolinite/illite. In addition to offering good storage space for free gas, this structure also offers good permeability and high surface area where the accessibility, gas transport, and diffusion rates are high for increased sorption of CO<sub>2</sub> either on clay or inertite (Karacan, 2003).

Porosity of the III–IV profile (Fig. 2-B) is generally 2–3% because of the expected low macroporosity of liptite, with some regional increases to 6–7% where mostly irregular mineral-filled fissures (Fig. 3-C) and intermittent pores in the maceral domain (Fig. 3-D) are present. Similarly, the porosity along the V–VI profile averages 2% (Fig. 2-C) because of low porosity of the vitrite–clarite domain. The SEM image taken at this location (Fig. 3-E) shows mineral patches with average compositions of 74.00% O, 8.03% Al, 0.40% Mg, 11.70% Si, 5.22% S, 0.60% K, and 0.30% Fe.

### 3.3. Evaluation of volumetric strains within the coal as a response CO<sub>2</sub> sorption

One goal of this paper is to demonstrate and to quantify volumetric strains occurring in confined and stressed coals as a response to sorption of CO<sub>2</sub>. This paper will also show how different microlithotypes are involved in this process. Previous work documented the linear and volumetric strain measurements of coal as a result of CO<sub>2</sub> sorption using different techniques, as presented in the Introduction section. However, it should be noted that almost all of these studies determined strains from the outside dimensions of the sample under zero effective stress. This may not represent the actual strain behaviors and magnitudes that may be occurring under elevated positive effective stresses, as seen in coalbed reservoirs. Moreover, the previous studies do not make any distinction between the microlithotypes and different sections of the sample.

The bulk density maps at the end of each CO<sub>2</sub> pressure increment were calculated using Eq. (1). Since the bulk density of coal masks the density increases (or decreases) in the actual coal material because of sorption of CO<sub>2</sub>, the maps were normalized using the density map of the initial coal. This enabled observations of only the changes within the coal. Fig. 4A, B, and C give the calculated bulk density maps at the end of each pressure regime (1.70, 3.06, 4.42 MPa).

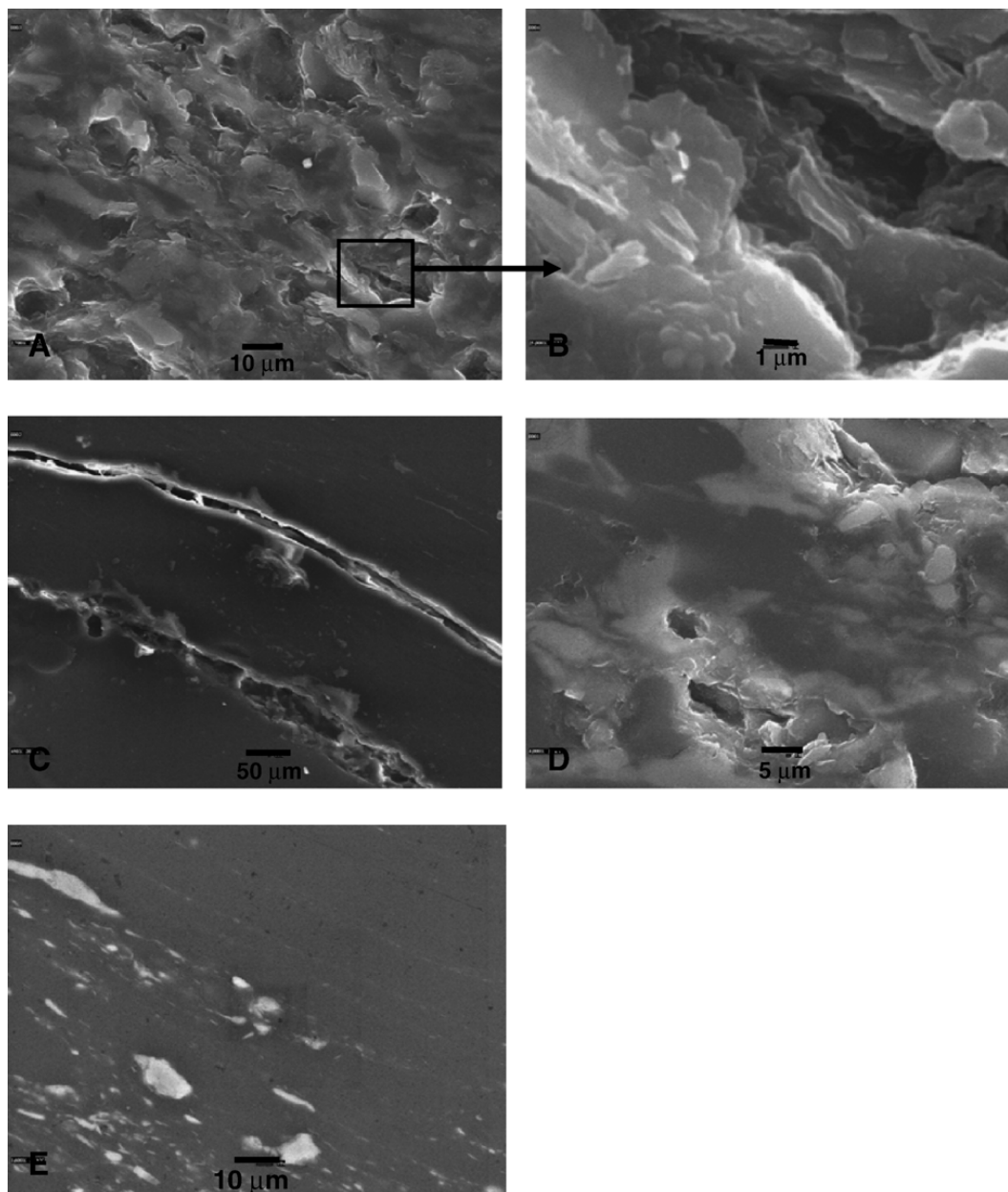


Fig. 3. SEM images taken at the clay and inertite layer (A and B), at a mostly liptite layer (C and D) and at a vitrite and clarite layer (E), using the polished section of the coal sample prepared from the scan location.

The bulk density maps given in Fig. 4 show that the clay + inertite regions (light colors in figures) can uptake a large amount of  $\text{CO}_2$ , and their densities may increase as much as 20% starting from the lower pressures up to 4.42 MPa. The clay type existing in these regions was identified as kaolinite and illite, as discussed in the previous section. These structures can uptake  $\text{CO}_2$  very rapidly because their porous and flaky nature creates high amounts of interlayer space, as evidenced by the SEM pictures and macroporosities. The fast pore diffusion enables gas molecules to penetrate into the macromolecular structure more easily. They are adsorbed on the large surface area of the clays, retained in the free

volume provided by the interlayer spaces of the clays, and absorbed by the inertite because of easy accessibility to these sites. Clays are known to provide high amounts of free space for fluid storage; however, there is not enough information about  $\text{CO}_2$  sorption on natural clays. In one study, Cimlerova and Arlt (2005) report a surprisingly high loading of the clays (montmorillonite and kaolinite) that they used in their  $\text{CO}_2$  adsorption studies.

On the other hand, Fig. 4A, B, and C show that most vitrite regions experienced a 6–10% density decrease compared to the initial density of the coal as a result of  $\text{CO}_2$  sorption. Since sorption is expected to increase the

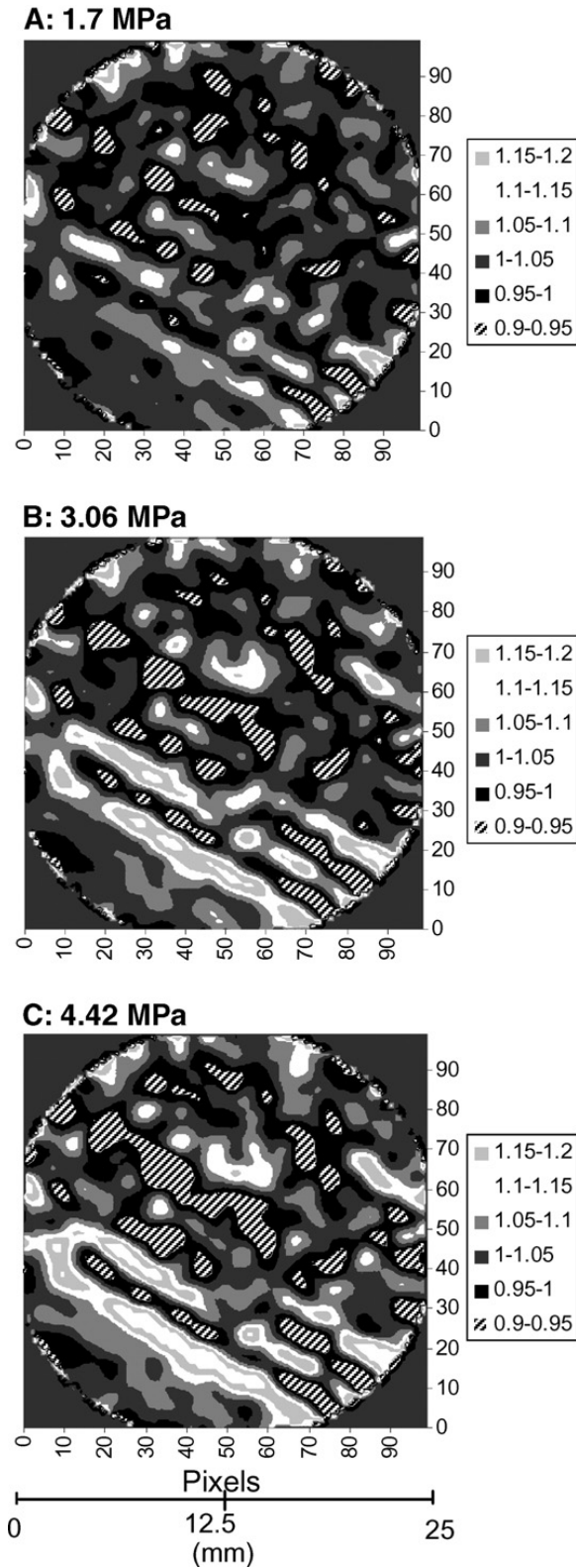


Fig. 4. Normalized bulk densities calculated within the coal using dual-energy computer tomography at the end of A: 1.70 MPa, B: 3.06 MPa and C: 4.42 MPa, CO<sub>2</sub> pressure, while the sample was under 1.36 MPa effective stress.

density of materials with fixed volumes, this density decrease can be explained by the swelling of vitrites as CO<sub>2</sub> dissolves in their cross-linked macromolecular

structure. Although the rearrangement is largely controlled by the coal, CO<sub>2</sub> acts as a plasticizer that adds additional free volume to the macromolecular network of glassy coal and lowers the  $T_g$  (glass transition temperature). This relaxation enables molecular rearrangements in the coal to a lower energy state. Carbon dioxide that is adsorbed and dissolved in the polymeric structure of vitrites allows the structure to relax or swell to conform to a new rubbery structure. Interestingly, this shows that confined coals also swell. However, swelling is more pronounced in vitrite and clarite-type microlithotypes compared to other microlithotypes that were present in the studied coal.

Density maps give a semi-quantitative rating of the amount of swelling, since density increase due to gas dissolution and density decrease due to volume increase counteract each other. The density data presented in Fig. 4A to C and the mass fractions of CO<sub>2</sub> ( $\omega_{CO_2}$ ) within the sample calculated using Eqs. (2), (4), and (5) were used to quantify volumetric strains. A mass balance over each image element (pixel) led to calculation of volumetric strains (defined as  $\Delta V/V$ ) as a function of time using the following equation:

$$\frac{\Delta V_{@t}}{V_{initial}}(x,y) = \frac{\rho_{initial}(x,y) - \rho_{@t}(x,y)}{\rho_{@t}(x,y)(1 - \omega_{CO_2@t}(x,y))} + \frac{\omega_{CO_2@t}(x,y)}{1 - \omega_{CO_2@t}(x,y)} \quad (7)$$

In this equation,  $\Delta V/V$  is the volumetric strain at any pixel location  $(x, y)$  in the coal at a particular time,  $t$ , during gas sorption.  $\omega_{CO_2}(x,y)$  is the mass percentage of CO<sub>2</sub> in the pixel  $(x,y)$  at time  $t$ ,  $\rho$  is the bulk density of coal.

The volumetric strain maps (as fractions) calculated using Eq. (7) are shown in Fig. 5A, B, and C at the equilibrium levels of each pressure step. Comparison of these maps with the internal structure image of the coal (Fig. 1) suggests that the coal matrix is mobile and rapidly exhibits more extensive swelling with increasing amounts of dissolved gas (increasing pressure), especially in the vitrite bands. These maps show that vitrite experienced 12.5–18.0% volumetric strain due to swelling at the end of 4.42 MPa pressure. The swelling-induced volumetric strains obtained for vitrites are close to the volumetric strains ( $\sim 16\%$ ) measured by Majewska and Zietek (in press), who used strain gauges for a bituminous coal sample from Poland during sorption of CO<sub>2</sub> at 4.0 MPa.

The maps presented in Fig. 5 also show that as swelling occurred, the clay and inertite layer was compressed to create space for the internal volume change in

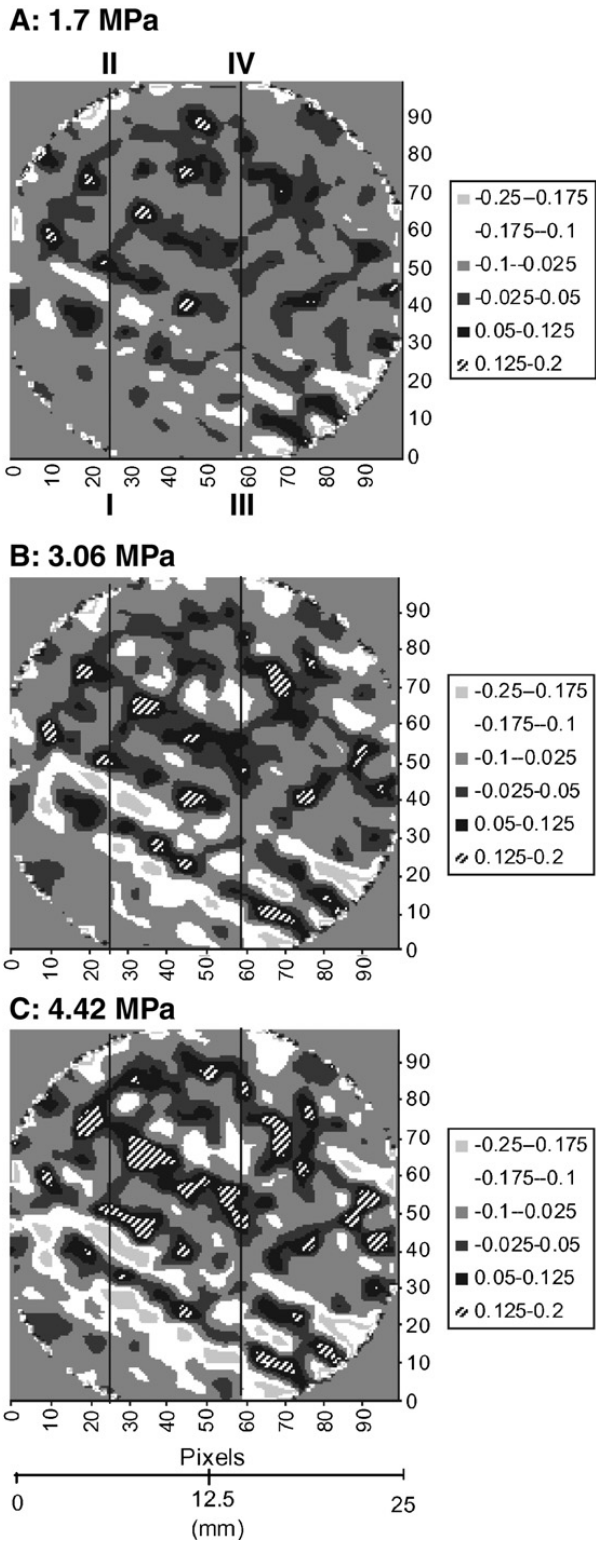


Fig. 5. Volumetric strain maps (in fractions) internal to the coal as a result of CO<sub>2</sub> sorption at the end of various CO<sub>2</sub> gas pressures (A: 1.70 MPa, B: 3.06 MPa, C: 4.42 MPa), while the sample was under 1.36 MPa effective stress. Vertical lines represent the profiles (I–II and III–IV) along different positions that have been used to extract the volumetric strain data presented in Fig. 6.

a closed system. The SEM images presented in Fig. 3A suggest that, in the case of clay layers, the pores and the interlayer spaces of the clay plates made this compression possible. Volumetric strain maps indicate that the amount of compression in clay and inertite layers was around 10.0–17.5%, which is very close to the volumetric strains created by swelling of vitrites, suggesting that the amount of compression was a reaction to swelling and was approximate in magnitude to the strains created by the vitrites. Volumetric strains (as compression) observed in the clay layer are also close to the calculated ~10–12% macroporosity, suggesting that the compression is made possible largely by the availability of macroporosity within kaolinite and inertite layers.

Fig. 6A and B present the volumetric strains along the profiles between I–II and III–IV shown in Fig. 5A to C for different gas pressures. The change of volumetric strains presented in these figures shows that the changes are quite variable within the sample based on the location and the pressure. In these plots, negative volumetric strains refer to the compressed regions, whereas positive volumetric strains refer to the swelling. The data in swollen locations show that the differential change in

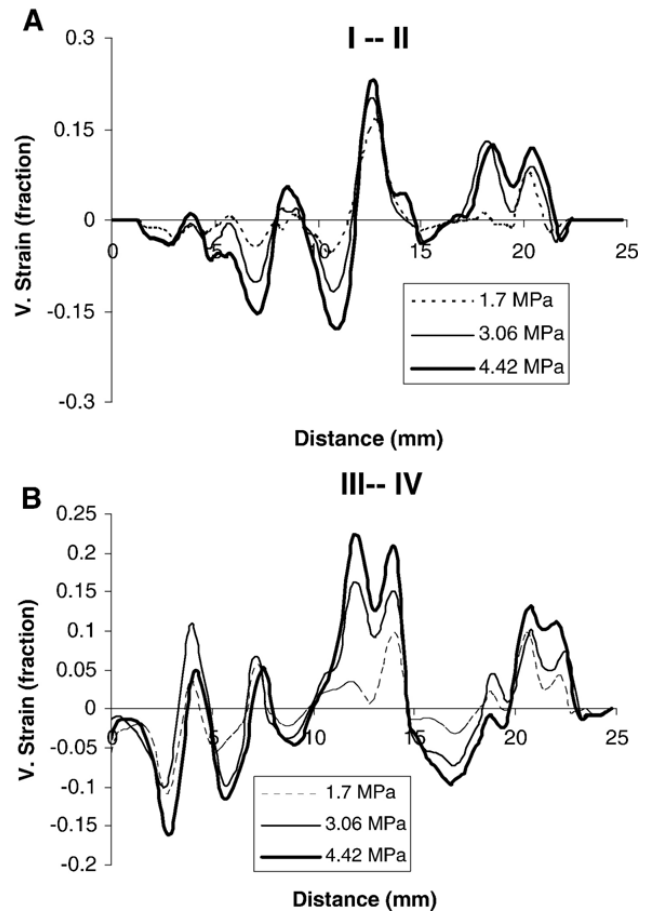


Fig. 6. Volumetric strain data (as fraction) extracted along the profiles shown in Fig. 5 as a function of location in the coal and CO<sub>2</sub> pressure.

volumetric strains associated with increased pressure may not be the same at different locations even if the identified microlithotypes are the same. The observed changes also show that the strains may not necessarily increase in a linear or Langmuir manner as pressure increases. This may be a consequence of spatial variations in local stresses experienced within the coal. These variations may change the local sorption characteristics and glass transition temperature depressions within the microlithotypes, resulting in changes in volumetric strain differentials of the same or similar microlithotypes between pressure increments. The effect of local stress variations on the volumetric strains occurring within the sample may be similar to the sorption and swelling behavior of polymers analyzed by [Wisinger and Paulaitis \(1987\)](#). They showed that at temperatures below  $T_g$ , the swelling and sorption behavior depend on the glass transition pressure ( $P_g$ ) in the presence of compressed  $\text{CO}_2$ . If the pressure corresponding to the maximum gas solubility is reached before  $P_g$ , then swelling and sorption level off and reach limiting values at elevated pressures. However, if  $P_g$  is less than the pressure corresponding to maximum gas solubility in the polymer, then sorption and swelling continue to increase with pressure and the effect of pressure on swelling is more pronounced than its effect on sorption.

It has been observed for polymers that hydrostatic pressure usually increases the glass transition temperature  $T_g$  of a polymer ([Bianchi, 1965](#); [Wang et al., 1982](#)). However, if the pressurizing medium is soluble in the polymer, a decrease in  $T_g$  with pressure is expected as the polymer is plasticized by the environment, as evidenced by both ultrasonic measurements of Young's modulus and static measurements of the creep compliance of the polymer ([Wang et al., 1982](#)). Thus, in the case of hydrostatically pressurized polymers, the interplay between the effect of solubility and the effect of pressure determines the onset of glass transition. The effect of constant confining stress or effective stress, on the coal during  $\text{CO}_2$  sorption has not been reported before. This study proves that confined coals also can swell due to  $\text{CO}_2$  dissolution in the coal matrix. However, it does not document the effect of different effective stress levels on swelling behavior. It has been suggested ([Karacan, 2003](#)) that confining pressure may favor the expulsion of extra  $\text{CO}_2$  by acting in the opposite direction to expansion in a confined volume, after the initial rapid swelling of coal due to structural rearrangements to a more stable structure in which solubility is reduced. A constant, prevailing, effective stress on the coal may also change the glass transition onset ( $T_g$  or  $P_g$ ) for rubberization and thus may also

change swelling by affecting the thermodynamic parameters. This is an important consideration for underground coal reservoirs in relation to gas transport and coal strength during  $\text{CO}_2$  injection.

The volumetric strain maps and graphical data in [Fig. 6](#) indicate that the volumetric strains within a coal sample during gas sorption are very heterogeneous and are functions of the local microlithotypes. The observed heterogeneity in swelling behavior within a consolidated and confined coal also suggests that a single sample may not be adequate for determining the impact of  $\text{CO}_2$  sorption on volumetric strain, especially if the sample lithology does not represent the average composition of the coalbed.

The implications of the calculated volumetric strain behavior can be significant for coalbed reservoir dynamics during a  $\text{CO}_2$  injection process or when  $\text{CO}_2$  intrusion occurs into the coalbed by natural processes, such as igneous activity or hydrodynamics. Since the clay layer was highly porous and probably very permeable, the compression imposed by swelling vitrites on the clay would likely decrease the permeability of the sample. If a similar process occurs in a reservoir where primary permeability is also controlled by clay veins, injectivity losses or permeability reductions may be inevitable.

The observed swelling behavior of a confined coal in response to  $\text{CO}_2$  sorption is based on the coal microlithotypes present. The restriction of permeable pathways in a swelled coalbed may have important implications for the occurrences of catastrophic gas outbursts in coal mines as well as injectivity losses experienced during enhanced coalbed methane production operations. Gas outbursts during underground coal mining generally associate with coalbeds of high gas content but with low permeabilities that lead to formation of high pressure gas pockets and with low mechanical strength ([Lama and Saghafi, 2002](#); [Li and Shimada, 2003](#)). [Li and Shimada \(2003\)](#) showed that coals in compressive environments and exhibiting tightly compressed and broken fractures with inefficient connectivity for gas flow to release gas pressure buildup were the most likely candidates for gas outbursts. These conditions can occur with swelling of coal matrix. [Ettinger and Serpinsky \(1991\)](#) showed that gas sorption changes the chemical potential of the coal and causes its swelling. Overburden pressure constrains the swelling, although internal forces lead to elevated internal pressures and compressions within the system. The swelling also increases the distance between coal atoms that decrease the mechanical strength of the coal. Mining of the coal changes the stress state of the coal and may lead to a sudden gas outburst.

### 3.4. Evaluation of CO<sub>2</sub> sorption

The strains created internally as a response to CO<sub>2</sub> sorption raise the question how much CO<sub>2</sub> was spatially

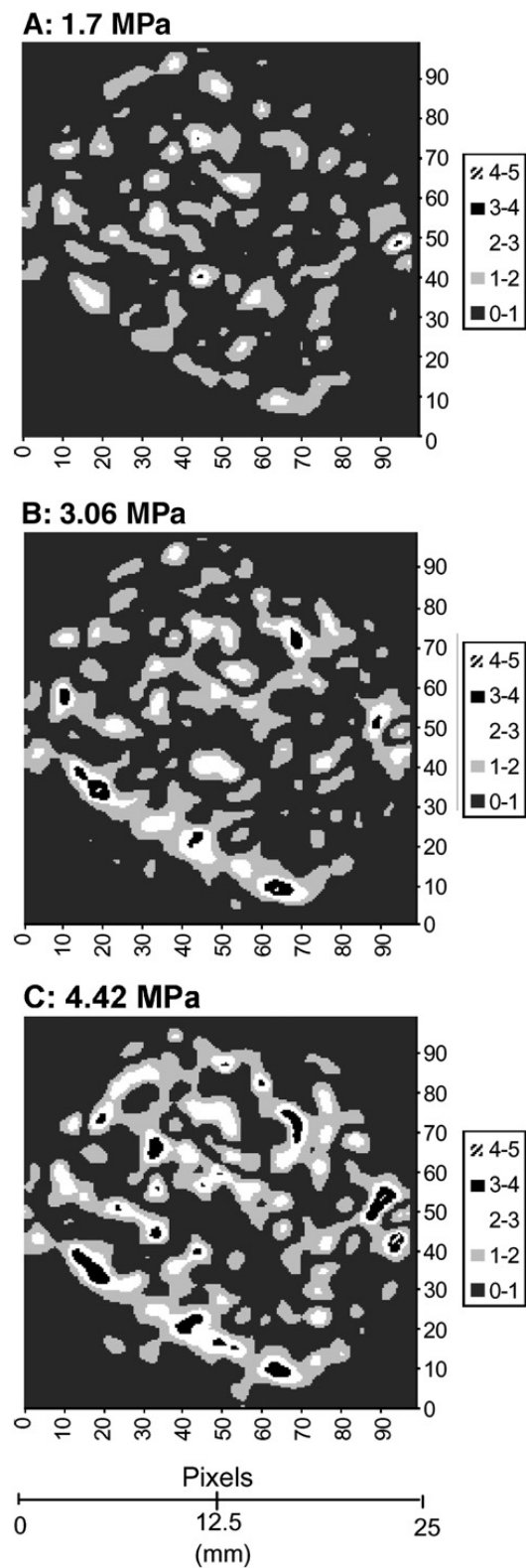


Fig. 7. CO<sub>2</sub> sorption amounts (in mmol/g) within the coal at the end of various CO<sub>2</sub> gas pressures (A: 1.70 MPa, B: 3.06 MPa, C: 4.42 MPa), while the sample was under 1.36 MPa effective stress.

sorbed within the coal. The computed total sorption amounts using image data were mapped (in mmol/g) in Fig. 7A to C for different CO<sub>2</sub> pressures. The maps show that the sorption amounts are variable within the sample, depending on the microlithotypes. The data indicate that most of the gas is retained by vitrite regions and by the clay and inertite layers. The amount of CO<sub>2</sub> sorbed by the vitrites is between 2 and 4 mmol/g, while the clay and inertite layers have comparable sorption capacity. Although it is not surprising that the vitrites can uptake high amounts of CO<sub>2</sub>, it is surprising to observe similar quantities for clay and inertites. There are insufficient data about CO<sub>2</sub> sorption on natural clays, other than the recent work of Cimlerova and Arlt (2005), who reported a surprising high loading of the clays (montmorillonite and kaolinite) in CO<sub>2</sub>. Based on the present work and the work of Cimlerova and Arlt (2005), it can be argued that the easy access of gas molecules to the high available surface areas of clays may be one of the factors that promote high sorption amounts. Particularly if the clays are mixed with the inertites, as in the case of the sample discussed in this paper, the flaky clay plates and the macroporosity they create will provide rapid access to inertites where CO<sub>2</sub> can be sorbed.

### 4. Conclusions

It has been demonstrated that confined coals swell during CO<sub>2</sub> sorption. The swelling is possibly due to dissolution and subsequent molecular rearrangements following the glass transition temperature depression. Swelling-induced volumetric strains are heterogeneous within the coal depending on the maceral composition of the coal material. It has been calculated that vitrites are the most-swelling lithotype, and the volumetric strains they create are in the order of 12.5–20.0% level at 4.42 MPa pressure. As the positive volumetric strains occur within the sample, they tend to compress any other region with higher porosity or any open fissures within the sample to create volume to expand. In this work, a clay and inertite layer, which had open pores and a highly porous flaky structure, was compressed. The amount of negative volumetric strains experienced by this layer was close to the amount of swelling.

Compression of high permeability clay bands, open fissures, and cleats within the coal is the reason for possible permeability reductions. Vitrites are the responsible lithotype group for this reduction because of the high volumetric strains they create upon CO<sub>2</sub> sorption.

Heterogeneity of calculated volumetric strains within the confined coal suggests that multiple samples should

be tested, possibly from different locations within the seam or even from the same block of coal in order to determine the volumetric strains as a response to gas sorption. Otherwise, calculated volumetric strains may not be representative of the coal seam being studied.

The calculated CO<sub>2</sub> sorption on different microlithotypes shows that the highest amount of sorption occurred on vitrites and on a clay–inertite layer (2–4 mmol/g). A possible explanation for the high amount of sorption on clay–inertite may be related to the SEM-evidenced structure of that layer: a porous, flaky, and possibly highly permeable structure enables fast gas transport and improved access to the large surface area provided by clay plates and inertite, where sorption can take place.

## Acknowledgements

Dr. J.W. Larsen is gratefully acknowledged for reviewing an earlier version of this paper and for making valuable comments. Dr. Isaac Zlochower of NIOSH is thanked for his help in SEM analysis.

## References

- Beamish, B.B., Crosdale, P.J., 1998. Instantaneous outbursts in underground coal mines: an overview and association with coal type. *International Journal of Coal Geology* 35, 27–55.
- Bianchi, U., 1965. Pressure effects on glass transition in polymers. *Journal of Physical Chemistry* 69, 1497–1504.
- Ceglarska-Stefanska, G., Czaplinski, A., 1993. Correlation between sorption and dilatometric processes in hard coals. *Fuel* 72, 413–417.
- Cimlerova, M., Arlt, W., 2005. Thermodynamics investigations for the adsorption of carbon dioxide on different rocks (abstract). AICHE Annual Meeting, Separation and CO<sub>2</sub> Capture for Sequestration III Session. Cincinnati, OH.
- Cody Jr., G.D., Larsen, J.W., Siskin, M., 1988. Anisotropic solvent swelling of coal. *Energy and Fuels* 2, 340–344.
- Duvauchelle, P., Peix, G., Babot, D., 1999. Effective atomic number in the Rayleigh to Compton scattering ratio. *Nuclear Instruments & Methods in Physics Research. Section B, Beam Interactions with Materials and Atoms* 155, 221–228.
- Ettinger, I.L., Serpinsky, V.V., 1991. On the state of methane in coal seams. *Mining Science and Technology* 13, 403–407.
- Gao, H., Masakutsa, N., Murata, S., Artok, L., 1999. Statistical distribution characteristics of pyridine transport in coal particles and a series of new phenomenological models for overshoot and nonovershoot solvent swelling of coal particles. *Energy and Fuels* 13, 518–528.
- Goodman, A.L., Favors, R.N., Hill, M.M., Larsen, J.W., 2005. Structure changes in Pittsburgh No. 8 coal caused by sorption of CO<sub>2</sub> gas. *Energy and Fuels* 19 (4), 1759–1760.
- Harpalani, S., Chen, G., 1995. Estimation in changes of fracture porosity of coal with gas emission. *Fuel* 74, 1491–1498.
- International Committee for Coal Petrology, 1963. *International Handbook of Coal Petrology*. Centre National de la Recherche Scientifique, Paris.
- Karacan, C.Ö., 2003. Heterogeneous sorption and swelling in a confined and stressed coal during CO<sub>2</sub> injection. *Energy and Fuels* 17 (6), 1595–1608.
- Karacan, C.Ö., Mitchell, G.D., 2003. Behavior and effect of different coal microlithotypes during gas transport for carbon dioxide sequestration into coal seams. *International Journal of Coal Geology* 4, 201–217.
- Kolak, J.J., Burruss, R.C., 2006. Geochemical investigation of the potential for mobilizing non-methane hydrocarbons during carbon dioxide storage in deep coal beds. *Energy and Fuels* 20 (2), 566–574.
- Lama, R., Saghafi, A., 2002. Overview of gas outbursts and unusual emissions. Third Australasian Coal Operators Conference. Wollongong, Australia.
- Larsen, J.W., 2004. The effects of dissolved CO<sub>2</sub> on coal structure and properties. *International Journal of Coal Geology* 57, 63–70.
- Larsen, J.W., Flowers II, R.A., Hall, P., Carlson, G., 1997. Structural rearrangement of strained coals. *Energy and Fuels* 11, 998–1002.
- Levine, J.R., 1996. Model study of the influence of matrix shrinkage on absolute permeability of coal bed reservoirs. In: Gayer, R., Harris, I. (Eds.), *Coalbed Methane and Coal Geology*, vol. 109. Geological Society Special Publication, London, pp. 197–212.
- Li, H.O., Shimada, S.Y., 2003. Mechanism of methane flow through sheared coals and its role on methane recovery. *Fuel* 82, 1271–1279.
- Majewska, Z., Zietek, J., in press. Changes of acoustic emission and strain in hard coal during gas sorption–desorption cycles. *International Journal of Coal Geology*.
- Özdemir, E., Morsi, B.I., Schroeder, K., 2003. Importance of volume effects to adsorption isotherms of carbon dioxide on coals. *Langmuir* 19 (23), 9764–9773.
- Palmer, I., Mansoori, J., 1998. How permeability depends on stress and pore pressure in coalbeds: a new model. *SPE Reservoir Evaluation and Engineering*, December, pp. 539–544.
- Pan, Z., Connell, L.D., 2007. A theoretical model for gas adsorption-induced coal swelling. *International Journal of Coal Geology* 69 (4), 243–252.
- Reeves, S., 2003. The COAL-SEQ project: results of the Allison and Tiffany ECBM field studies. *Proceedings of 2nd Annual DOE/NETL Conf. on Carbon Sequestration*, Alexandria, VA.
- Reucroft, P.J., Sethuraman, A.R., 1987. Effect of pressure on carbon dioxide induced coal swelling. *Energy and Fuels* 1, 72–75.
- Robertson, E.P., Christiansen, R.L., 2005. Measurement of sorption induced strain. Paper 0532, *Proceedings of the 2005 International Coalbed Methane Symposium*, Tuscaloosa, AL.
- Romanov, V.N., Goodman, A.L., Larsen, J.W., 2006a. Errors in CO<sub>2</sub> adsorption measurements caused by coal swelling. *Energy and Fuels* 20 (1), 415–416.
- Romanov, V., Soong, Y., Schroeder, K., 2006b. Volumetric effects in coal sorption capacity Measurements. *Chemical Engineering and Technology* 29, 368–374.
- Schätzler, H.P., 1979. Basic aspects on the use of elastic and inelastic scattered gamma radiation for the determination of binary systems with effective atomic numbers of less than 10. *International Journal of Applied Radiation and Isotopes* 30, 115–121.
- Wang, W.-C.V., Kramer, E.J., Sachse, W.H., 1982. Effects of high-pressure CO<sub>2</sub> on the glass transition temperature and mechanical properties of polystyrene. *Journal of Polymer Science. Polymer Physics Edition* 20 (8), 1371–1384.
- Wissinger, R.G., Paulaitis, M.E., 1987. Swelling and sorption in polymer–CO<sub>2</sub> mixtures at elevated pressures. *Journal of Polymer Science. Part B, Polymer Physics* 25, 2497–2510.